ACS APPLIED MATERIALS & INTERFACES

Research Article

www.acsami.org

Hierarchical Core–Shell Structure of ZnO Nanorod@NiO/MoO_2 Composite Nanosheet Arrays for High-Performance Supercapacitors

Sucheng Hou,[†] Guanhua Zhang,[†] Wei Zeng,[†] Jian Zhu,[†] Feilong Gong,[‡] Feng Li,[‡] and Huigao Duan*[,†]

[†]College of Physics and Microelectronics, State Key Laboratory for Chemo/Biosensing and Chemometrics, Hunan University, Hunan 410082, China

[‡]State Laboratory of Surface and Interface Science and Technology, Zhengzhou University of Light Industry, Zhengzhou 450002, China

Supporting Information

ABSTRACT: A hierarchical core–shell structure of ZnO nanorod@NiO/MoO_2 composite nanosheet arrays on nickel foam substrate for high-performance supercapacitors was constructed by a two-step solution-based method involving two hydrothermal processes followed by a calcination treatment. Compared to one composed of pure NiO/MoO_2 composite nanosheets, the hierarchical core–shell structure electrode displays better pseudocapacitive behaviors in 2 M KOH, including high areal specific capacitance values of 1.18 F cm^{-2} at 5 mA cm^{-2} and 0.6 F cm^{-2} at 30 mA cm^{-2} as well as relatively good rate capability at high current densities. Furthermore, it also shows remarkable cycle stability, remaining at 91.7% of the initial value even after 4000 cycles at a current density of 10 mA cm^{-2}. The enhanced pseudocapacitive behaviors are mainly due to the unique hierarchical core–shell structure and the synergistic effect of combining ZnO nanorod arrays and NiO/MoO_2 composite nanosheets. This novel hierarchical core–shell structure shows promise for use in next-generation supercapacitors.

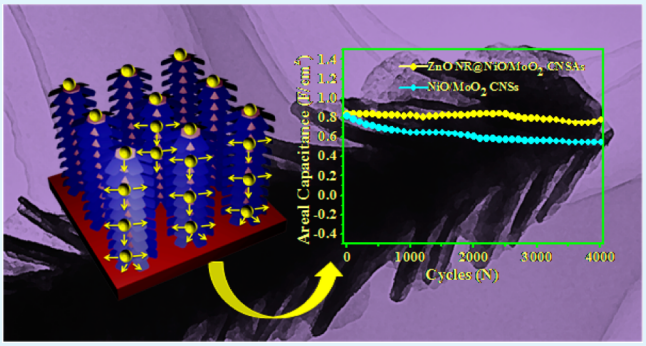

KEYWORDS: *supercapacitors, ZnO nanorod arrays, NiO/MoO_2 composite nanosheets, core–shell structure*

INTRODUCTION

Lightweight, low-cost, and safe energy storage devices with the ability to rapidly store abundant electrical energy may play a key role in addressing the problems of climate change and the limited availability of fossils fuels, as well as for the efficient storage of solar and wind energy.[1−6] Among various energy storage devices, pseudocapacitors (PCs) have attracted significant attention due to their excellent performance, such as high energy densities, fast charge–discharge characteristics, long life cycle, and ability to bridge between traditional capacitors and batteries/fuel cells.[7−9] However, compared to electrical double-layer capacitors (EDLCs), they exhibit poor rate capability and inferior cycle ability, which limit their further applications.[10,11] Thus, it is of significant importance to rationally design electrode structures or synthesize electrode materials with high specific capacitance, good rate capability, and cycle stability for the development of PCs.

In order to enhance pseudocapacitive performance, different materials have been investigated as the electrodes in PCs, such as RuO_2, NiO, Fe_2O_3, SnO_2, and MoO_2.[12−17] Among them, RuO_2 has exhibited ultrahigh specific capacitance and excellent reversibility, but it is not widely used in commerce due to its high cost and rarity in nature.[18,19] Recently, nanocomposite materials have drawn considerable attention, as they can provide better characteristics than the single materials.[20−26] For example, Zhong et al.[25] demonstrated a Co_3O_4/$Ni(OH)_2$ nanocomposite material with a high specific capacitance of 684 F g^{-1}, which is higher than those of $Ni(OH)_2$ (113 F g^{-1}) and Co_3O_4 (161 F g^{-1}). Wang et al.[24] reported a $NiCo_2O_4$/SWCNT nanocomposite that exhibited better cycle stability than $NiCo_2O_4$. However, although the nanocomposite materials indeed have improved specific capacitance, they still show other shortcomings. For instance, the previous Co_3O_4/$Ni(OH)_2$ nanocomposite materials displayed a bad cycle stability, losing 36% of the initial capacitance only after 500 cycles, while the reported $NiCo_2O_4$/SWCNT nanocomposite showed poor rate capability, and its capacitance decayed rapidly with increasing current density. The most likely reason may be the poor electronic conductivity of metal oxides.

To solve this problem, carbon nanomaterials, which possess large surface area and good electrical conductivity, have been used as supporters to grow active materials.[27−29] However, these carbon supporters could suffer severe corrosion in the electrochemical window of some metal oxides.[30] Such corrosion will cause the active materials to fall from the supporters and agglomerate in the substrate, leading to fast

Received: May 8, 2014
Accepted: August 5, 2014
Published: August 5, 2014

   dx.doi.org/10.1021/am5028154 | ACS Appl. Mater. Interfaces 2014, 6, 13564−13570

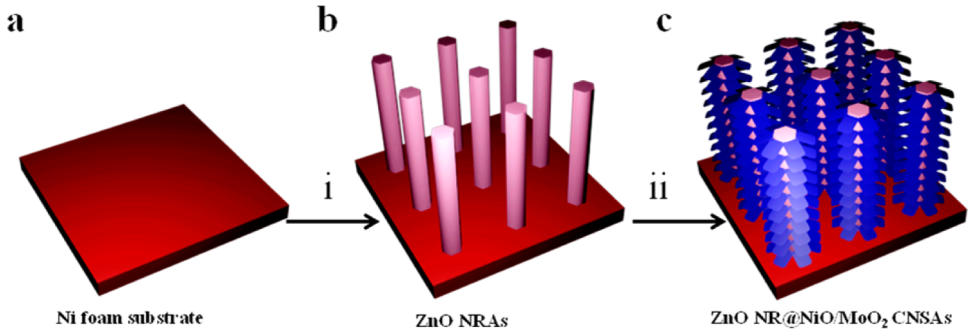

Figure 1. Schematic illustration of the fabrication processes of ZnO NR@NiO/MoO_2 CNSAs hierarchical heterostructures: (a) Ni foam substrate; (b) ZnO NRAs on Ni foam substrate; (c) hierarchical core–shell structure of ZnO NR@NiO/MoO_2 CNSAs.

degradation of the electrochemical performance of the active electrodes. Recently, ZnO nanorods (NRs) have drawn increasing attention and have been demonstrated as good scaffolds to support active materials due to their excellent characteristics such as low capacity, large specific surface area, chemical stability, and good electrical conductivity.[31−35] Futhermore, they can also provide short diffusion paths for ions and facilitate electron transfer. Therefore, it is extremely reasonable to use ZnO NRs as a scaffold to grow metal oxide nanocomposite materials, so as to construct a novel hierarchical core–shell structure.

In this work, we have prepared a novel hierarchical core–shell structure of ZnO nanorod@NiO/MoO_2 composite nanosheet arrays (ZnO NR@NiO/MoO_2 CNSAs) on Ni foam for supercapacitor applications via a two-step solution route followed by a calcination treatment. We use NiO and MoO_2 as the active materials in consideration of their multiple valence states, environmentally benign nature, affordable cost, and natural abundance. On one hand, the ZnO nanorod arrays (NRAs) can serve as a scaffold, providing large surface area for the growth of NiO/MoO_2 composite nanosheets (CNSs) and also avoiding the conventional aggregation of the active materials that degrades the cycle stability. On the other hand, the NiO/MoO_2 CNSs possess large specific surface area and multiple oxide sites, which can be beneficial for the improvement of areal specific capacitance (ASC). For example, this novel hierarchical core–shell structure of ZnO NR@NiO/MoO_2 CNSAs exhibits a high ASC of 1.18 F cm^{-2} at the current density of 5 mA cm^{-2}, and excellent cycle stability with 91.7% retention after 4000 cycles at the current density of 10 mA cm^{-2}. Thus, with this novel hierarchical core–shell structure, ZnO NR@NiO/MoO_2 CNSAs on Ni foam can be expected to be promising candidates for supercapacitor applications.

EXPERIMENTAL SECTION

Preparation of ZnO NRAs on Ni Foam. In this experiment, all the chemicals were analytical grade and were used without further purification. Ahead of the experiment, the Ni foam substrate (1 × 1 cm^2) was ultrasonically washed with ethanol and water for 20 min each and then placed into the autoclave liners vertically. The reaction solution was prepared by mixing 0.015 M zinc nitrate hexahydrate and 0.015 M hexamethylenetetraamine (HMTA) together with 2 mL of ammonia in 70 mL of distilled water under constant magnetic stirring for 30 min. The reaction solution was then transferred into the autoclave liners and kept sealed at 90 °C for 24 h. After the reaction, the Ni foam coated with a white product was washed with deionized water, and thus the ZnO NRAs were obtained.

Preparation of ZnO NR@NiO/MoO_2 CNSAs. The ZnO NRAs prepared as described above were used as the scaffold for the growth of NiO/MoO_2 CNSs via a facile hydrothermal method. First, 0.018 g of $Ni(NO_3)_2{\cdot}H_2O$ and 0.015 g of $Na_2MoO_4{\cdot}7H_2O$ were dissolved in 50 mL of distilled water under constant magnetic stirring for 30 min. Second, the above solution was transferred into autoclave liners, and the as-prepared ZnO NRAs substrate was immersed into the reaction solution. Finally, the solution was sealed in a stainless steel autoclave and maintained at 150 °C for 1 h. After the reaction, in order to remove the residuals, the Ni foam substrate with light green color was washed with deionized water for a few minutes and then dried at 60 °C for 12 h. Afterward, the sample was annealed at 400 °C for 1 h in pure argon, and thus the ZnO NR@NiO/MoO_2 CNSAs were obtained. For comparison, we also prepared pure NiO/MoO_2 CNSs directly on Ni foam substrate (1 × 1 cm^2) using the same method under the same conditions.

Characterizations. The surface morphologies of the ZnO NR@NiO/MoO_2 CNSAs were characterized by field-emission scanning electron microscopy (FESEM, Hitachi S-4800) with an operating voltage of 15 kV, and high-resolution transmission electron microscopy (HRTEM, JEOL JEM-2100) with an accelerating voltage of 200 kV. The powders scraped off from the Ni foam substrate were characterized by X-ray diffraction (XRD, Rigaku D/Max-2550 with Cu Kα radiation).

Electrochemical Measurements. Electrochemical properties of ZnO NR@NiO/MoO_2 CNSAs and pure NiO/MoO_2 CNSs were studied with cyclic voltammetry (CV), charge–discharge measurements, and electrochemical impedance spectroscopy (EIS) tests in an electrochemical workstation (CHI660E, Shanghai, Chenhua) using a three-electrode electrochemical configuration in 2 M KOH aqueous solution. The ZnO NR@NiO/MoO_2 CNSA (1 × 1 cm^2, ZnO NRAs mass = 2 mg, NiO/MoO_2 CNSs mass = 1.2 mg) or pure NiO/MoO_2 CNS (1 × 1 cm^2, NiO/MoO_2 CNSs mass = 1.2 mg) was directly used as the working electrode. A platinum electrode was used as counter electrode, and a saturated calomel electrode (SCE) was used as reference electrode.

RESULTS AND DISCUSSION

Our method for preparing the hierarchical core–shell structure of ZnO NR@NiO/MoO_2 CNSAs as pseudocapacitive electrode involved two key steps, as shown in Figure 1. The first step was to synthesize ZnO NRAs on the Ni foam substrate via a hydrothermal method (Figure 1a,b). The second step was to grow NiO/MoO_2 CNSs on the surfaces of ZnO NRAs through another hydrothermal method followed by a calcination process. After the two steps, the hierarchical core–shell structure of ZnO NR@NiO/MoO_2 CNSAs was constructed on the Ni foam substrate, as shown in Figure 1c.

The successful preparation of ZnO NR@NiO/MoO_2 CNSAs on Ni foam substrate was first confirmed by powder XRD. We know that the Ni foam substrate has strong XRD peak signals;

therefore, in order to exclude them, the powders for XRD analysis were scraped off from the Ni foam substrate. Figure 2

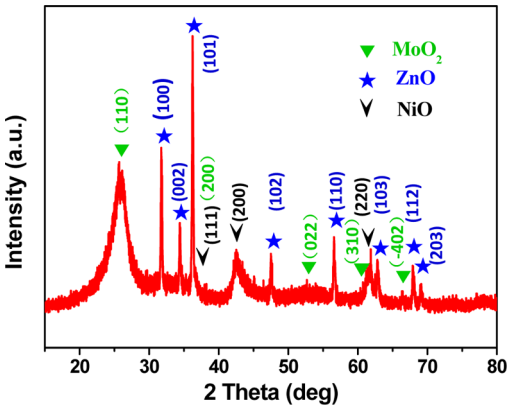

Figure 2. XRD pattern of the ZnO NR@NiO/MoO_2 CNSAs.

shows the XRD pattern of the ZnO NR@NiO/MoO_2 CNSAs. It is obvious that all the diffraction peaks of the powders can be indexed to the standard diffraction patterns of ZnO (JCPDS no. 79-2205), NiO (JCPDS no. 65-2901), and MoO_2 (JCPDS no. 73-1249), and there are no impurity peaks detected. It should be mentioned that the appearance of relatively weak peak intensity for NiO and MoO_2 is mainly due to the presence of ZnO, which displays stronger XRD peaks.

In order to determine the molar ratio of Ni/Mo, X-ray energy dispersive spectroscopy (EDS) was carried out in transmission electron microscopy (TEM) to study the percentage composition of the sample (Supporting Information, Figure S6). The result shows that the atomic content of Ni/Mo is 2.38 and 1.16, respectively; according to this result, the molar ratio of Ni/Mo is ~2.

Figure 3 shows the scanning electron microscopy (SEM) images of the ZnO NRAs and ZnO NR@NiO/MoO_2 CNSAs. As shown in Figure 2a, free-standing and well-aligned ZnO NRs are grown on Ni foam substrate through the hydrothermal process, forming ZnO NRAs. ZnO NRs are hexagonal, having a uniform diameter of ~300 nm (inset of Figure 3b) and a uniform length of ~4 μm (Figure 3b). After another hydrothermal process, followed by a calcination treatment, ZnO NRs were decorated with hierarchical NiO/MoO_2 CNSs, and the diameter increased to ~600 nm (Figure 3c,d). The NiO/MoO_2 CNSs were sequentially and firmly grown on the surface of ZnO NRAs, forming a scale-like surface morphology (Figure 3d), which can be beneficial for electrolytes to fully penetrate into the active materials, improving the specific capacitance. In contrast, the pure NiO/MoO_2 CNSs were casually and irregularly grown on the Ni foam substrate (Supporting Information, Figure S1).

To further study the morphology and structure of the resultant ZnO NR@NiO/MoO_2 CNSA core–shell structures, TEM investigations were carried out. Figure 4a shows a typical bright-field TEM image at low magnification for the sample. It is clearly observed that the nanorod is composed of a ZnO NR "core" and a NiO/MoO_2 CNS "shell", and the ZnO NRs are well wrapped with the scale-like ultrathin NiO/MoO_2 CNSs, forming a typical core–shell structured nanorod. The length of the NiO/MoO_2 CNSs is ~150 nm. Figure 4b,c shows HRTEM images taken from the shell of ZnO NR@NiO/MoO_2 CNSAs. Evidently, the thickness of NiO/MoO_2 CNSs is only ~20 nm

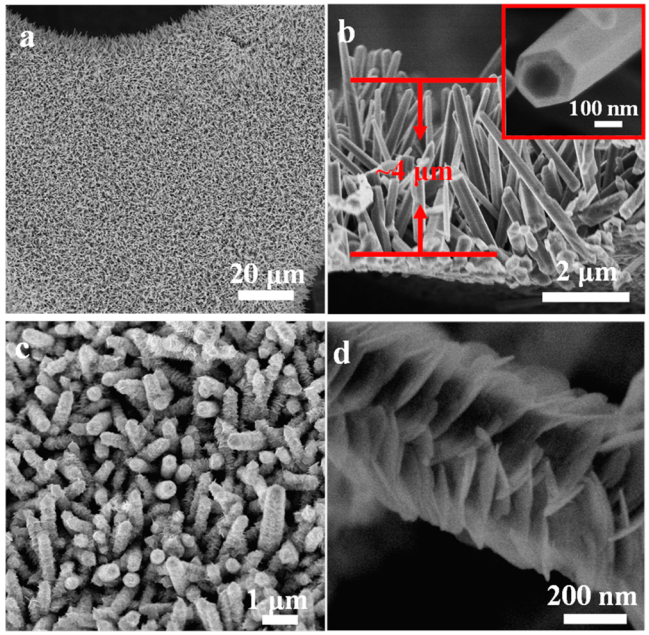

Figure 3. Scanning electron microscopy (SEM) characterization of the samples. (a) SEM image of ZnO NRAs on Ni foam. (b) SEM image of side-view ZnO NRAs. The inset shows an enlarged image of a ZnO NR. (c) SEM image of ZnO NR@NiO/MoO_2 CNSAs. (d) High-magnification SEM image of ZnO NR@NiO/MoO_2 CNSAs.

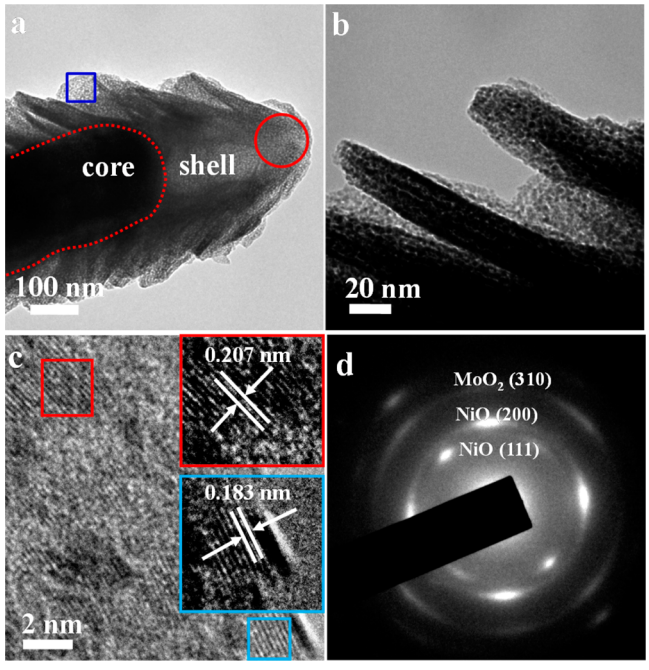

Figure 4. Transmission electron micrography (TEM) characterization of the samples. (a) TEM image of ZnO NR@NiO/MoO_2 CNSAs core–shell structure. (b) HRTEM image taken from the edge of ZnO NR@NiO/MoO_2 CNSAs. (c) HRTEM image taken from the blue square in (a). (d) SAED image taken from the red circle in (a).

and the gap between two neighboring NiO/MoO_2 CNSs is ~40 nm (Figure 4b), meaning that all the NiO/MoO_2 CNSs on the surface of ZnO NRs are active materials that can participate in the redox reaction and no "dead" or "inactive" materials exist. Furthermore, the NiO/MoO_2 CNSs have reasonable crystallinity, with lattice spacings of 0.207 and

dx.doi.org/10.1021/am5028154 | ACS Appl. Mater. Interfaces 2014, 6, 13564–13570

0.183 nm, corresponding to the distance of NiO (200) and MoO_2 (−122), respectively (Figure 4c). As expected, the selected-area electron diffraction (SAED) pattern (Figure 4d) taken from the NiO/MoO_2 CNS shell (corresponding to the red circle in Figure 4a) shows a set of concentric rings, which indicates the polycrystalline nature of the NiO/MoO_2 CNSs, and the diffraction rings from outside to inside can be indexed to the planes of (310) MoO_2, (200) NiO, and (111) NiO, respectively. The TEM results are well in agreement with the observed XRD pattern.

The complicated growth process of the shell structure of ZnO NR@NiO/MoO_2 CNSAs can be reasonably explained by "self-assembly" and "oriented attachment". During the oriented attachment process, neighboring particles share a common crystallographic orientation through spontaneous self-organization, and then they capture other particles at the planar interface. After this process, the particles reduce their overall energy and bond together by sacrificing the surface energy associated with the unsatisfied bonds.[36,37] In this reaction, ZnO NRs play the role of a backbone to guide the self-assembly of the CNSs without using surfactant and stabilizers. The nanoparticles then grow according to the "oriented attachment" mechanism and can also attach to the surface of ZnO to decrease surface energy due to the high surface energy and thermodynamic instability. As shown in Figure S2 in the Supporting Information, as the reaction time increased, more nanoparticles attached to the surface of ZnO, forming nanosheets gradually. After a calcination treatment, the hierarchical core−shell structure of ZnO NR@NiO/MoO_2 CNSAs was finally formed.

To investigate the electrochemical performance of ZnO NR@NiO/MoO_2 CNSAs, the sample of ZnO NR@NiO/MoO_2 CNSAs supported on Ni foam (1 × 1 cm^2) was used directly as an integrated electrode and measured in a three-electrode mode with 2 M KOH as the electrolyte. Figure 5a shows the typical CV curves of the ZnO NR@NiO/MoO_2 CNSAs electrode with different scan rates, ranging from 10 to 200 mV s^{-1}. It is obvious that all the CV curves have a pair of strong redox peaks, indicating that the capacitance characteristics of the ZnO NR@NiO/MoO_2 CNSAs electrode were mainly dominated by Faradaic redox reactions. MoO_2 has been demonstrated to have electrochemical capacities similar to those of MnO_2,[38,39] which means that MoO_2 principally shows EDLC characteristics in this experiment. Therefore, the Faradaic redox reactions were mainly caused by reactions of Ni (ii) ↔ Ni (iii) + e^-. Besides, on one hand, the shape of the CV curves is not significantly changed, although the scan rates ranged from 10 to 200 mV s^{-1}, which means that the mass transportation and electron conduction in the host materials were greatly improved by the introduction of ZnO NRs. The corresponding CV curves of the pure NiO/MoO_2 CNSs electrode are shown in Figure S3 (Supporting Information). On the other hand, the current increases with increasing scan rate, and the cathodic and anodic peaks move to negative and positive potential, respectively, keeping their position symmetrical at the same time. This reveals that the materials can undergo a high current charge−discharge process and exhibit excellent reversibility.

For comparison, Figure 5b shows the CV curves of the ZnO NR@NiO/MoO_2 CNSAs electrode and the pure NiO/MoO_2 CNSs electrode at a scan rate of 40 mV s^{-1}. As can be seen, the enclosed area of the pure NiO/MoO_2 CNSs electrode is much smaller than that of the ZnO NR@NiO/MoO_2 CNSAs

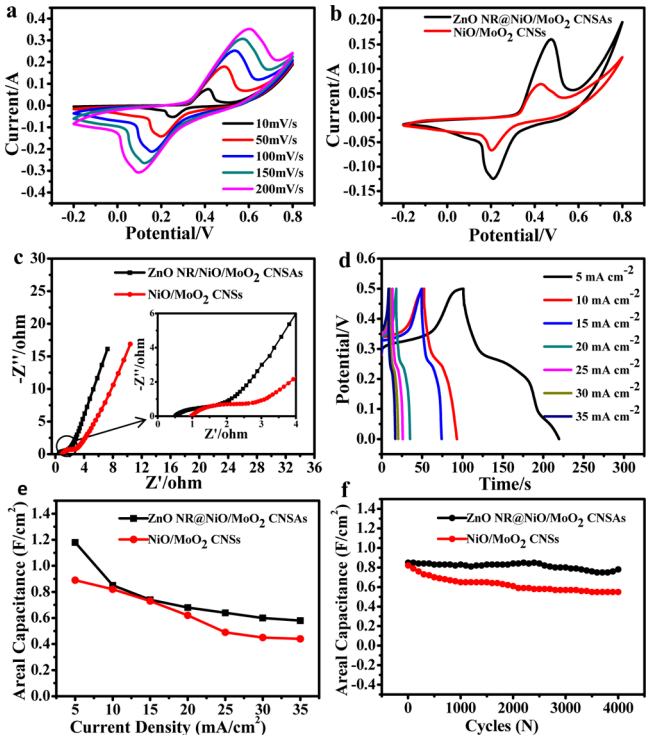

Figure 5. Electrochemical performance of the hierarchical core−shell structure. (a) CV curves of the ZnO NR@NiO/MoO_2 CNSAs on Ni foam at different scan rates. (b) Comparison of ZnO NR@NiO/MoO_2 CNSAs and pure NiO/MoO_2 CNSs at the same scan rate of 40 mV s^{-1}. (c) Impedance Nyquist plots of ZnO NR@NiO/MoO_2 CNSAs and pure NiO/MoO_2 CNSs at open-circuit potential. (d) CP curves of the ZnO NR@NiO/MoO_2 CNSAs on Ni foam at different current densities. (e) ASC of the two electrodes as a function of current density. (f) ASC as a function of cycle number of the ZnO NR@NiO/MoO_2 CNSAs and pure NiO/MoO_2 CNSs electrodes between 0 and 0.5 V at a current density of 10 mA cm^{-2}.

electrode, which indicates that the ZnO NR@NiO/MoO_2 CNSAs electrode exhibits a higher ASC. This result is probably due to the advantages of the 3D structure of ZnO NRAs, which can increase the contact surface between the active materials and the electrolyte and facilitate ion diffusion and electron transfer.

The improved ion diffusion and electron transfer behaviors were further confirmed by EIS measurements of the two electrodes, and the corresponding Nyquist plots are shown in Figure 5c. From the plots, we can learn that the ZnO NR@NiO/MoO_2 CNSAs hierarchical core−shell structure displays lower Warburg impedance (W), bulk resistance, and charge-transfer resistance than pure NiO/MoO_2 CNSs (inset of Figure 5c). The reduced Faraday resistance caused by the 3D structure of ZnO NRAs leads to the shorter ion path, enhanced electrochemical reaction, and higher ASC value of ZnO NR@NiO/MoO_2 CNSAs hierarchical core−shell structure.

Galvanostatic charge−discharge measurements were performed at various current densities over a potential range of 0−0.5 V to get further information about the capacitive properties of the ZnO NR@NiO/MoO_2 CNSAs electrode. Figure 5d shows the charge−discharge profiles at different current densities from 5 to 35 mA cm^{-2}. Evidently, there is a distinct plateau region in each charge or discharge process, suggesting the capacitance derives from redox reaction and exhibits typical pseudocapacitive characteristics, which is in line with the CV

dx.doi.org/10.1021/am5028154 | ACS Appl. Mater. Interfaces 2014, 6, 13564−13570

curves (Figure 5a). The ASC of the ZnO NR@NiO/MoO_2 CNSAs electrode and the pure NiO/MoO_2 CNSs is calculated from the discharge times according to the following formula:

$$C_s = \frac{I\Delta t}{S\Delta V}$$

where C_s (F cm^{-2}) is areal specific capacitance, I (A) represents the discharge current, and S (cm^2), ΔV (V) and Δt (s) designate the area of the electrode, potential drop during discharge, and total discharge time, respectively.

The calculated results are collected in Figure 5e. The ASC values of the ZnO NR@NiO/MoO_2 CNSAs electrode are 1.18, 0.85, 0.74, 0.68, 0.64, 0.6, and 0.58 F cm^{-2} at the current densities of 5, 10, 15, 20, 25, 30, and 35 mA cm^{-2}, respectively, while those of the pure NiO/MoO_2 CNSs electrode are 0.89, 0.81, 0.72, 0.62, 0.49, 0.45, and 0.44 F cm^{-2}. When the ASC is converted into gram-specific capacitance, the values for the ZnO NR@NiO/MoO_2 CNSAs electrode are 983, 708, 617, 567, 533, 500, and 483 F g^{-1} at the current densities of 4.16, 8.33, 12.15, 16.68, 20.82, 25.00, and 29.10 A g^{-1}, respectively, while those of the pure NiO/MoO_2 CNSs electrode are 742, 683, 608, 516, 408, 375, and 367 F g^{-1} at the current densities of 4.15, 8.43, 12.66, 16.64, 20.82, 25.00, and 29.23 A g^{-1}, respectively. It is noticeable that the ZnO NR@NiO/MoO_2 CNSAs electrode delivers higher ASC and better rate capability at high current densities than the pure NiO/MoO_2 CNSs electrode. In order to get an intuitive comparison, the first and the 4000th charge−discharge curves are shown in Figure S4 (Supporting Information). It is obvious that after 4000 cycles there is a severe decrease for the pure NiO/MoO_2 CNSs electrode (Figure S4a) but just a slight decrease in the ZnO NR@NiO/MoO_2 CNSAs electrode (Figure S4b), which demonstrates that after long-time cycling, the hierarchical core−shell structure of ZnO NR@NiO/MoO_2 CNSAs still maintained good electrochemical reversibility. The improved rate capability of the ZnO NR@NiO/MoO_2 CNSAs electrode can be attributed to the special roles of the inner 3D ZnO NRAs core structure. This structure served as a scaffold, providing a large surface area for the growth of NiO/MoO_2 CNSs which thus avoided the conventional aggregation of the active materials, and functioned as an efficient electron-conducting pathway.

In addition, the superior performance of the ZnO NR@NiO/MoO_2 CNSAs electrode is further manifested by its outstanding cycle stability. Figure 5f depicts the cycle stability of the pure NiO/MoO_2 CNSs and ZnO NR@NiO/MoO_2 CNSAs electrodes over 4000 cycles from 0 to 0.5 V at a current density of 10 mA cm^{-2}. It is observed that the cycle stability is greatly enhanced in the ZnO NR@NiO/MoO_2 CNSAs electrode. It shows a high ASC of 0.78 F cm^{-2} after 4000 cycles and keeps 91.7% of the initial value of 0.85 F cm^{-2} at the current density of 10 mA cm^{-2}, much higher than the pure electrode (0.55 F cm^{-2} with 67.9%). This result proves that the combination of nanocomposite metal oxides materials with the ZnO NRs largely improves the rate capability and the cycle stability of the nanocomposite metal oxide materials.

Futhermore, to the best of our knowledge, these electrochemical results for the ZnO NR@NiO/MoO_2 CNSAs are better than those for the porous ZnO/NiO composite micropolyhedrons (649 F g^{-1} at 5.8 A g^{-1}),[40] the single-crystal ZnO NR with nanoporous NiO shell composite (305 F g^{-1} at 10 mV s^{-1}),[41] and the ordered mesoporous MoO_2 (146 F g^{-1} at 5 mv $^{-1}$ and 90% retention after 1000 cycles at 1 A g^{-1}).[39] Such excellent performance of the ZnO NR@NiO/MoO_2 CNSAs electrode further proves the great advantages of the 3D hierarchical core−shell structure.

Several factors can account for the high ASC, good rate capability, and excellent cycle stability of the ZnO NR@NiO/MoO_2 CNSAs. First, there may be a synergistic contribution due to the hierarchical core−shell structure of the ZnO NR@NiO/MoO_2 CNSAs. On one hand, the 3D structure of ZnO NRAs served as a scaffold, providing a large surface area for the growth of NiO/MoO_2 CNSs and accelerating electron transport for the Faradaic reaction. On the other hand, the NiO/MoO_2 CNSs possessed large specific surface area and multiple oxide sites, which can improve specific capacitance and provide more electronic transmission channels (as schematically illustrated in Figure 6). Second, the gap between the neighboring NiO/MoO_2 CNSs made the electrolyte fully penetrate into the inner region of the electrode, increasing the utilization of the active materials. Third, the ZnO NRs were grown directly on the Ni foam substrate with a robust adhesion, avoiding the use polymer binders, which reduced the amount of "dead" or "inactive" materials and facilitated the ion diffusion and electron transfer, improving the rate capability. Most importantly, the ZnO NRs possess the characteristics of chemical stability and good electrical conductivity and are tightly integrated with the NiO/MoO_2 CNSs, making the structure stable and strengthening the structural integrity of the core during the charge−discharge process, resulting in enhanced cycle stability.

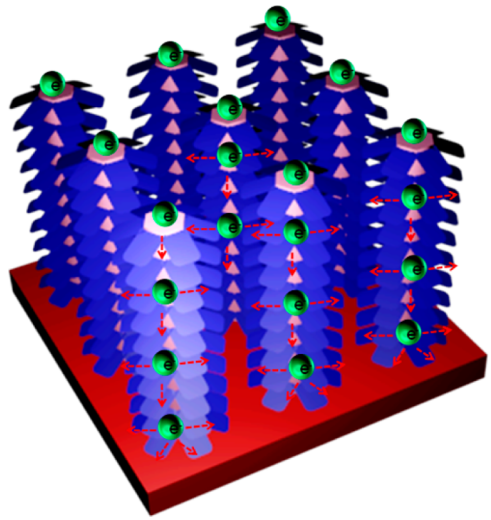

Figure 6. Electron transportation mechanism of the ZnO NR@NiO/MoO_2 CNSAs, in which both ZnO NRAs scaffolds and NiO/MoO_2 CNSs provide channels for electron transport.

CONCLUSIONS

In summary, a novel hierarchical core−shell structure of ZnO NR@NiO/MoO_2 CNSAs was successfully prepared by a facile method in this study. It has been demonstrated that the combination of ZnO NRs and NiO/MoO_2 CNSs exhibits excellent electrochemical performance with a high ASC of 1.18 F cm^{-2} at the current density of 5 mA cm^{-2} and better rate capability at high current densities than pure NiO/MoO_2 CNSs. It also shows remarkable cycle stability, which remains at 91.7% of the initial value even after 4000 cycles at the current density of 10 mA cm^{-2}. Such attractive capacitive behaviors are

attributed to the unique hierarchical core−shell structure and the synergistic effects of the combination of ZnO NRs and NiO/MoO_2 CNSs. The excellent electrochemical capacitive performance, low cost, and easy preparation of the ZnO NR@NiO/MoO_2 CNSs make them promising materials for supercapacitor applications.

■ ASSOCIATED CONTENT

Supporting Information

SEM of the as-prepared pure NiO/MoO_2 CNSs, SEM of the ZnO NR@NiO/MoO_2 CNSAs with different reaction times, SEM of the ZnO NR@NiO/MoO_2 CNSAs after 4000th cycles, CV curves of the pure NiO/MoO_2 CNSs on Ni foam at scan rates from 10 to 200 mV/s, the first and the 4000th charge−discharge curves of the two electrodes, and EDS of the ZnO NR@NiO/MoO_2 CNSAs. This material is available free of charge via the Internet at http://pubs.acs.org.

■ AUTHOR INFORMATION

Corresponding Author

*E-mail: duanhg@hnu.edu.cn.

Notes

The authors declare no competing financial interest.

■ ACKNOWLEDGMENTS

We gratefully acknowledge financial support from the National Natural Science Foundation of China (grant nos. 11274107 and 61204109), the Program for New Century Excellent Talents in University (NCET-13-0185), and the Foundation for the authors of National Excellent Doctoral Dissertation of China (201318). F.L. thanks the National Natural Science Foundation of China (grant nos. 21071130 and 21371157) and Key Program of Henan Province for Science and Technology (132102210424) for support.

■ REFERENCES

(1) Merlet, C.; Rotenberg, B.; Madden, P. A.; Taberna, P. L.; Simon, P.; Gogotsi, Y.; Salanne, M. On the Molecular Origin of Supercapacitance in Nanoporous Carbon Electrodes. *Nat. Mater.* **2012**, *11*, 306−310.

(2) Cao, Y. B.; Xiao, Y. H.; Gong, Y. Y.; Wang, C. F.; Li, F. One-pot Synthesis of MnOOH Nanorods on Graphene for Asymmetric Supercapacitors. *Electrochim. Acta* **2014**, *127*, 200−207.

(3) Tarascon, J. M.; Armand, M. Issues and Challenges facing Rechargeable Lithium Batteries. *Nature* **2001**, *414*, 359−367.

(4) Jiang, H.; Lee, P. S.; Li, C. Z. 3D Carbon Based Nanostructures for Advanced Supercapacitors. *Energy Environ. Sci.* **2013**, *6*, 41−53.

(5) Simon, P.; Gogotsi, Y. Materials for Electrochemical Capacitors. *Nat. Mater.* **2008**, *7*, 845−854.

(6) Winter, M.; Brodd, R. J. What are Batteries, Fuel Cells, and Supercapacitors? *Chem. Rev.* **2004**, *104*, 4245−4270.

(7) Largeot, C.; Portet, C.; Chmiola, J.; Taberna, P. L.; Gogotsi, Y.; Simon, P. Relation between the Ion Size and Pore Size for an Electric Double-Layer Capacitor. *J. Am. Chem. Soc.* **2008**, *130*, 2730−2731.

(8) Wang, G. P.; Zhang, L.; Zhang, J. J. A Review of Electrode Materials for Electrochemical Supercapacitors. *Chem. Soc. Rev.* **2012**, *41*, 797−828.

(9) Kandalkar, S.; Dhawale, D.; Kim, C. K.; Lokhande, C. Chemical Synthesis of Cobalt Oxide Thin Film Electrode for Supercapacitor Application. *Synth. Met.* **2010**, *160*, 1299−1302.

(10) Hercule, K. M.; Wei, Q. L.; Khan, A. M.; Zhao, Y. L.; Tian, X. C.; Mai, L. Q. Synergistic Effect of Hierarchical Nanostructured $MoO_2/Co(OH)_2$ with largely Enhanced Pseudocapacitor Cyclability. *Nano Lett.* **2013**, *13*, 5685−5691.

(11) Sharma, P.; Bhatti, T. A Review on Electrochemical Double-Layer Capacitors. *Energy Convers. Manage.* **2010**, *51*, 2901−2912.

(12) Tang, C. H.; Tang, Z.; Gong, H. Hierarchically Porous Ni-Co Oxide for High Reversibility Asymmetric Full-Cell Supercapacitors. *J. Electrochem. Soc.* **2012**, *159*, A651−A656.

(13) Xia, H.; Meng, Y. S.; Yuan, G. L.; Cui, C.; Lu, L. A Symmetric RuO_2/RuO_2 Supercapacitor Operating at 1.6 V by using a Neutral Aqueous Electrolyte. *Electrochem. Solid-State Lett.* **2012**, *15*, A60−A63.

(14) Zhang, Y. J.; Sun, C. T.; Lu, P.; Li, K. Y.; Song, S. Y.; Xue, D. F. Crystallization Design of MnO_2 towards Better Supercapacitance. *CrystEngComm* **2012**, *14*, 5892−5897.

(15) Wang, W. J.; Hao, Q. L.; Lei, W.; Xia, X. F.; Wang, X. Graphene/SnO_2/Polypyrrole Ternary Nanocomposites as Supercapacitor Electrode Materials. *RSC Adv.* **2012**, *2*, 10268−10274.

(16) Gao, F. L.; Zhang, L. J.; Huang, S. M. Fabrication Horizontal Aligned MoO_2/Single-Walled Carbon Nanotube Nanowires for Electrochemical Supercapacitor. *Mater. Lett.* **2010**, *64*, 537−540.

(17) Xia, X. F.; Hao, Q. L.; Lei, W.; Wang, W. J.; Sun, D. P.; Wang, X. Nanostructured Ternary Composites of Graphene/Fe_2O_3/Polyaniline for High-Performance Supercapacitors. *J. Mater. Chem.* **2012**, *22*, 16844−16850.

(18) Hu, C. C.; Chang, K. H.; Lin, M. C.; Wu, Y. T. Design and Tailoring of the Nanotubular Arrayed Architecture of Hydrous RuO_2 for next Generation Supercapacitors. *Nano Lett.* **2006**, *6*, 2690−2695.

(19) Wei, T. Y.; Chen, C. H.; Chien, H. C.; Lu, S. Y.; Hu, C. C. A Cost-Effective Supercapacitor Material of Ultrahigh Specific Capacitances: Spinel Nickel Cobaltite Aerogels from an Epoxide-Driven Sol-Gel Process. *Adv. Mater.* **2010**, *22*, 347−351.

(20) Ding, L. X.; Wang, A. L.; Li, G. R.; Liu, Z. Q.; Zhao, W. X.; Su, C. Y.; Tong, Y. X. Porous Pt-Ni-P Composite Nanotube Arrays: Highly Electroactive and Durable Catalysts for Methanol Electrooxidation. *J. Am. Chem. Soc.* **2012**, *134*, 5730−5733.

(21) Lu, X. H.; Huang, X.; Xie, S. L.; Zhai, T.; Wang, C. S.; Zhang, P.; Yu, M. H.; Li, W.; Liang, C. L.; Tong, Y. X. Controllable Synthesis of Porous Nickel-Cobalt Oxide Nanosheets for Supercapacitors. *J. Mater. Chem.* **2012**, *22*, 13357−13364.

(22) Xiao, Y. H.; Liu, S. J.; Li, F.; Zhang, A. Q.; Zhao, J. H.; Fang, S. M.; Jia, D. Z. Hierarchical Nanoarchitectures: 3D Hierarchical Co_3O_4 Twin-Spheres with an Urchin-Like Structure: Large-Scale Synthesis, Multistep-Splitting Growth, and Electrochemical Pseudocapacitors. *Adv. Funct. Mater.* **2012**, *22*, 4051−4051.

(23) Mao, L.; Zhang, K.; Chan, H. S. O.; Wu, J. S. Nanostructured MnO_2/Graphene Composites for Supercapacitor Electrodes: the Effect of Morphology, Crystallinity and Composition. *J. Mater. Chem.* **2012**, *22*, 1845−1851.

(24) Wang, X.; Han, X. D.; Lim, M. F.; Singh, N.; Gan, C. L.; Jan, M.; Lee, P. S. Nickel Cobalt Oxide-Single Wall Carbon Nanotube Composite Material for Superior Cycling Stability and High-Performance Supercapacitor Application. *J. Phys. Chem. C* **2012**, *116*, 12448−12454.

(25) Zhong, J. H.; Wang, A. L.; Li, G. R.; Wang, J. W.; Ou, Y. N.; Tong, Y. X. $Co_3O_4/Ni(OH)_2$ Composite Mesoporous Nanosheet Networks as a Promising Electrode for Supercapacitor Applications. *J. Mater. Chem.* **2012**, *22*, 5656−5665.

(26) Wang, Z.; Chen, T.; Chen, W. X.; Chang, K.; Ma, L.; Huang, G. C.; Chen, D. Y.; Lee, J. Y. CTAB-Assisted Synthesis of Single-Layer MoS_2-Graphene Composites as Anode Materials of Li-Lon Batteries. *J. Mater. Chem. A* **2013**, *1*, 2202−2210.

(27) Zhi, M. J.; Xiang, C. C.; Li, J. T.; Li, M.; Wu, N. Q. Nanostructured Carbon-Metal Oxide Composite Electrodes for Supercapacitors: A Review. *Nanoscale* **2013**, *5*, 72−88.

(28) Lee, S. W.; Kim, J.; Chen, S.; Hammond, P. T.; Shao-Horn, Y. Carbon Nanotube/Manganese Oxide Ultrathin Film Electrodes for Electrochemical Capacitors. *ACS Nano* **2010**, *4*, 3889−3896.

(29) Fischer, A. E.; Pettigrew, K. A.; Rolison, D. R.; Stroud, R. M.; Long, J. W. Incorporation of Homogeneous, Nanoscale MnO_2 within Ultraporous Carbon Structures via Self-Limiting Electroless Deposition: Implications for Electrochemical Capacitors. *Nano Lett.* **2007**, *7*, 281−286.

(30) Huang, S. Y.; Ganesan, P.; Park, S.; Popov, B. N. Development of a Titanium Dioxide-Supported Platinum Catalyst with Ultrahigh Stability for Polymer Electrolyte Membrane Fuel Cell Applications. *J. Am. Chem. Soc.* **2009**, *131*, 13898−13899.
(31) Trang, N. T. H.; Van Ngoc, H.; Lingappan, N.; Kang, D. J. A Comparative Study of Supercapacitive Performances of Nickel Cobalt Layered Double Hydroxides Coated on ZnO Nanostructured Arrays on Textile Fibre as Electrodes for Wearable Energy Storage Devices. *Nanoscale* **2014**, *6*, 2434−2439.
(32) Yang, P. H.; Xiao, X.; Li, Y. Z.; Ding, Y.; Qiang, P. F.; Tan, X. H.; Mai, W. J.; Lin, Z. Y.; Wu, W. Z.; Li, T. Q. Hydrogenated ZnO Core-Shell Nanocables for Flexible Supercapacitors and Self-Powered Systems. *ACS Nano* **2013**, *7*, 2617−2626.
(33) Liu, J. P.; Cheng, C. W.; Zhou, W. W.; Li, H. X.; Fan, H. J. Ultrathin Nickel Hydroxidenitrate Nanoflakes Branched on Nanowire Arrays for High-Rate Pseudocapacitive Energy Storage. *Chem. Commun.* **2011**, *47*, 3436−3438.
(34) Wang, Z. L.; Guo, R.; Li, G. R.; Lu, H. L.; Liu, Z. Q.; Xiao, F. M.; Zhang, M.; Tong, Y. X. Polyaniline Nanotube Arrays as High-Performance Flexible Electrodes for Electrochemical Energy Storage Devices. *J. Mater. Chem.* **2012**, *22*, 2401−2404.
(35) Wang, Z. L.; Zhu, Z. L.; Qiu, J. H.; Yang, S. H. High Performance Flexible Solid-State Asymmetric Supercapacitors from MnO_2/ZnO Core-Shell Nanorods//Specially Reduced Graphene Oxide. *J. Mater. Chem. C* **2014**, *2*, 1331−1336.
(36) Mai, L. Q.; Yang, F.; Zhao, Y. L.; Xu, X.; Xu, L.; Luo, Y. Z. Hierarchical $MnMoO_4$/$CoMoO_4$ Heterostructured Nanowires with Enhanced Supercapacitor Performance. *Nat. Commun.* **2011**, *2*, 381−381.
(37) Zhang, G. H.; Wang, T. H.; Yu, X. Z.; Zhang, H. N.; Duan, H. G.; Lu, B. A. Nanoforest of Hierarchical Co_3O_4@$NiCo_2O_4$ Nanowire Arrays for High-Performance Supercapacitors. *Nano Energy* **2013**, *2*, 586−594.
(38) Qu, Q. T.; Zhang, P.; Wang, B.; Chen, Y. H.; Tian, S.; Wu, Y. P.; Holze, R. Electrochemical Performance of MnO_2 Nanorods in Neutral Aqueous Electrolytes as a Cathode for Asymmetric Supercapacitors. *J. Phys. Chem. C* **2009**, *113*, 14020−14027.
(39) Li, X. Y.; Shao, J.; Li, J.; Zhang, L.; Qu, Q. T.; Zheng, H. H. Ordered Mesoporous MoO_2 as a High-Performance Anode Material for Aqueous Supercapacitors. *J. Power Sources* **2013**, *237*, 80−83.
(40) Pang, H.; Ma, Y. H.; Li, G. C.; Chen, J.; Zhang, J. S.; Zheng, H. H.; Du, W. M. Facile Synthesis of Porous ZnO-NiO Composite Micropolyhedrons and their Application for High Power Supercapacitor Electrode Materials. *Dalton Trans.* **2012**, *41*, 13284−13291.
(41) He, Y. B.; Li, G. R.; Wang, Z. L.; Su, C. Y.; Tong, Y. X. Single-Crystal ZnO Nanorod/Amorphous and Nanoporous Metal Oxideshell Composites: Controllable Electrochemical Synthesis and Enhanced Supercapacitor Performances. *Energy Environ. Sci.* **2011**, *4*, 1288−1292.